Published in Solar Energy Materials and Solar Cells 81, issue 1, 61-71, 2004
which should be used for any reference to this work

Relationship between Raman crystallinity and open-circuit voltage in microcrystalline silicon solar cells

C. Droz*, E. Vallat-Sauvain, J. Bailat, L. Feitknecht, J. Meier, A. Shah

Institute of Microtechnology, University of Neuchâtel, Breguet 2, Neuchâtel 2000, Switzerland

Abstract

A series of nip-type microcrystalline silicon (μc-Si:H) single-junction solar cells has been studied by electrical characterisation, by transmission electron microscopy (TEM) and by Raman spectroscopy using 514 and 633 nm excitation light and both top- and bottom-illumination. Thereby, a Raman crystallinity factor indicative of crystalline volume fraction is introduced and applied to the interface regions, i.e. to the mixed amorphous-microcrystalline layers at the top and at the bottom of entire cells. Results are compared with TEM observations for one of the solar cells. Similar Raman and electrical investigations have been conducted also on pin-type μc-Si:H single-junction solar cells. Experimental data show that for all nip and pin μc-Si:H solar cells, the open-circuit voltage linearly decreases as the average of the Raman crystallinity factors for top and bottom interface regions increases.

Keywords: Solar cells; Microcrystalline silicon; Raman spectroscopy; Crystallinity; Open-circuit voltage

1. Introduction

Hydrogenated microcrystalline silicon (μc-Si:H) is known to be a complex material consisting of crystalline and amorphous silicon (a-Si:H) phases plus grain boundaries. This material exhibits a wide range of microstructures that depend both on the deposition conditions [1,2] and on the substrate material [3]. In particular, one

*Corresponding author. Tel.: +41-32-718-3312; fax: +41-32-718-3201.
E-mail address: corinne.droz@unine.ch (C. Droz).

of the key deposition parameters is the silane content in the plasma gas phase. Indeed, μc-Si:H is obtained by diluting silane (SiH_4) in hydrogen (H_2). By decreasing the silane concentration $SC = SiH_4/(SiH_4 + H_2)$ down to a few percent, the material undergoes an a-Si:H/μc-Si:H transition. The value of SC used for the deposition of the intrinsic (i) layer has been shown to play a significant role in determining the highest so far attainable values for the open-circuit voltage (V_{oc}) of a pin cell [4]. On the other hand, it is well known that the material microstructure depends as well on silane concentration [1,5]. At present, the best electrical performances are achieved for μc-Si:H solar cells with their i-layer deposited near the transition [6,7]. Under these conditions, the microstructure of μc-Si:H varies in the course of the growth process of the i-layer: a fully amorphous incubation layer is generally observed for the initial growth region (i.e. for the bottom) of the layers, followed, thereafter, by a microcrystalline phase; the latter consists of conical conglomerates made up of crystallites of a few tens of nanometres size [8].

Micro-Raman spectroscopy is a fast and non-destructive tool utilised for the monitoring of crystallinity. The interest of this tool is that it gives us the basic possibility to characterise the volume fractions of amorphous and crystalline phases within actual (functioning) solar cells, and that we are able to measure the electrical performances (and particularly the V_{oc}-value) on the very same solar cells.

In this paper, we are conducting bifacial Raman measurements, i.e. we are illuminating the cell first from the top and then from the bottom side; thereby we can evaluate selectively the n–i or the p–i interface. We are also using two different source-light wavelengths (514 and 633 nm), so that we thus obtain depth-dependant information. From each of these four Raman spectra, a "Raman crystallinity factor" is then calculated by evaluating the scattered intensities assigned to amorphous and microcrystalline silicon. The evolution of these different Raman crystallinity factors is observed here for a series of nip-type solar cells where the silane concentration used for the deposition of the intrinsic layer has been varied. As a countercheck, a transmission electron microscopy (TEM) micrograph for a typical solar cell from this series is analysed. Furthermore, several pin-type solar cells are also evaluated with the same specific technique of Raman spectroscopy. Finally, all solar cells are electrically characterised and a link between the V_{oc}-value and the Raman crystallinity factor is demonstrated for both nip- and pin-configurations.

2. Experimental

Microcrystalline silicon solar cells in the nip- and pin-configurations were deposited by the very high frequency glow discharge (VHF-GD) technique, at plasma excitation frequencies between 70 and 130 MHz, on glass substrates (AF45 Schott) coated with various types of transparent conducting oxides (TCO), namely in-house low-pressure chemical vapour deposited (LP-CVD) zinc oxide (ZnO) and in-house sputtered ZnO, as well as commercial tin oxide (SnO_2), without any metallic back reflector. In particular, two series of nip cells were deposited simultaneously on sputtered ZnO and LP-CVD ZnO, respectively, with the same

"highly microcrystalline" deposition conditions (low value of SC) for the n- and p-layers. The SC used for deposition of the i-layers was varied from 5% (highly microcrystalline material) to 7% (mixed phase (μc-Si:H/a-Si:H) material). The i-layer thicknesses all ranged between 2.0 and 2.5 μm. More details on these cells can be found in Refs. [8,9]. In addition to these two series of nip-cells, some other nip cells not pertaining to these series, as well as a large set of pin cells (that can be considered to be typical products of our solar cell technology laboratory at IMT Neuchâtel) which cover a wide range of V_{oc} values (see Ref. [4]) were also analysed both electrically and by Raman spectroscopy.

A commercial Renishaw Raman imaging microscope (System 2000) functioning in backscattering configuration and equipped with a long working-distance objective was operated at two different wavelengths: with the strongly absorbed 514 nm line of an Ar laser and with the weakly absorbed 633 nm line of a HeNe laser. Micro-Raman experiments were performed on the solar cells in two ways: with focused excitation light arriving *either* through the TCO on the top, last-deposited silicon layer of the device (i.e. on the p-layer for the nip devices, and on the n-layer for the pin devices), *or* through the glass substrate and the TCO on the bottom, first-deposited silicon layer of the device. For each solar cell, both wavelengths were applied in each focusing configuration, resulting in four "bifacial, depth-dependent" Raman spectra for each solar cell.

A few samples from the series of nip cells described above were prepared as cross-section [8,10] for TEM observation on a Philips CM200 microscope operated at 200 kV.

3. Results and discussion

3.1. Raman and TEM observations

On each solar cell we measured the electrical performances and probed the crystallinity by determining the bifacial depth-dependent Raman spectra described above. Typical results for the four Raman spectra are given in Fig. 1.

The Raman spectra in the range from 360 to 580 cm^{-1} were then deconvoluted with three Gaussian peaks and a quadratic baseline, with an algorithm based on the Levenberg–Marquardt method [11], as illustrated in Fig. 1d. These three peaks are attributed to the different phases present in the sample. First, the narrow line centred at about 520 cm^{-1} (which is the position of the transverse optic (TO) mode in crystalline silicon (c-Si)) is attributed to silicon crystallites. In our samples, it exhibits a maximum centred at a mean value of $518 \pm 1\ cm^{-1}$, and has a mean full-width at half-maximum (FWHM) value of $10 \pm 1\ cm^{-1}$. This peak frequently exhibits a tail towards smaller wavenumbers (around 510 cm^{-1}): a tail that has, in the literature, been attributed either to crystallites of diameters lower than 10 nm [12], or to a silicon Wurzite phase [13], that could result from twinning defects [2]. In our deconvolution procedure, this tail is fitted with a peak at 510 cm^{-1}, bounded between 505 and 515 cm^{-1} (in order to avoid a competition between the 510 cm^{-1} and the

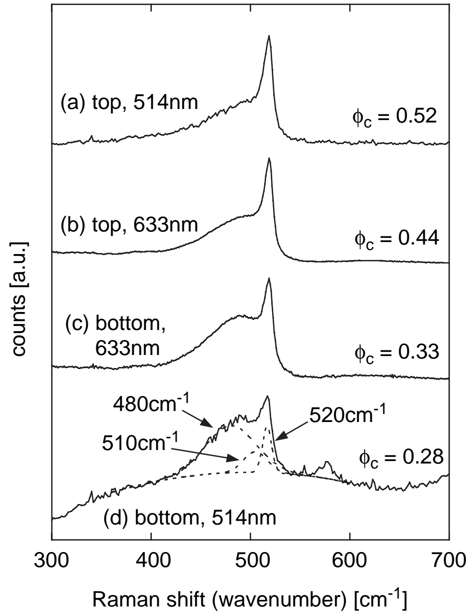

Fig. 1. Bifacial depth-dependent Raman spectra of a nip-type solar cell with its i-layer deposited at SC = 7% on sputtered ZnO. The TEM micrograph of this cell is given in Fig. 2. The spectra are recorded from the top side (ZnO/p-layer) (a and b) and from the bottom side (glass/ZnO/n-layer) (c and d), with 514 nm (a and d) and 633 nm (b and c) excitation light. The three peaks, centred, respectively, at 520 cm^{-1} (crystalline phase), 510 cm^{-1} (defective crystalline phase) and 480 cm^{-1} (amorphous phase), as used for the deconvolution, are shown as dotted lines on spectrum d. Note that even if an important background signal due to the luminescence of the glass is present in the bottom focusing configuration (d), it does not hinder the measurement and the interpretation of the spectra. The Raman crystallinity factor ϕ_c extracted from each spectrum (see text) is also given.

480 cm^{-1} peaks during the fit, as observed in Ref. [14]), and which has a mean FWHM value of 26 ± 2 cm^{-1}. In the following part of this work, the 510 cm^{-1} peak will be attributed to the defective part of the crystalline phase and will be included in the crystalline fraction. Finally, a broad peak fixed in our deconvolution procedure at 480 cm^{-1} (mean FWHM value of 53 ± 7 cm^{-1}), is characteristic of the TO mode in a-Si:H, and thus attributed to the amorphous silicon phase.

The Raman signal collected in the micro-Raman experiment is equal to the integral, taken over the excited volume, of the depth distribution of each phase [15]. The excited volume depends on the penetration depth of the laser light used. The penetration depth at 514 nm is of the order of 100 nm for a-Si:H and of 300 nm for μc-Si:H, whereas at 633 nm it reaches about 1 μm for both materials [16]. However, in our experimental backscattering set-up, the collected Raman light is scattered from half of these depths [15,17]. This results in a characteristic Raman collection depth (RCD) (see Fig. 2) ranging from about 50 nm (within a-Si:H) to about 150 nm (within μc-Si:H), for the 514 nm excitation light. For the 633 nm excitation light, RCD equals about 500 nm within all the silicon-based layers. These depths are

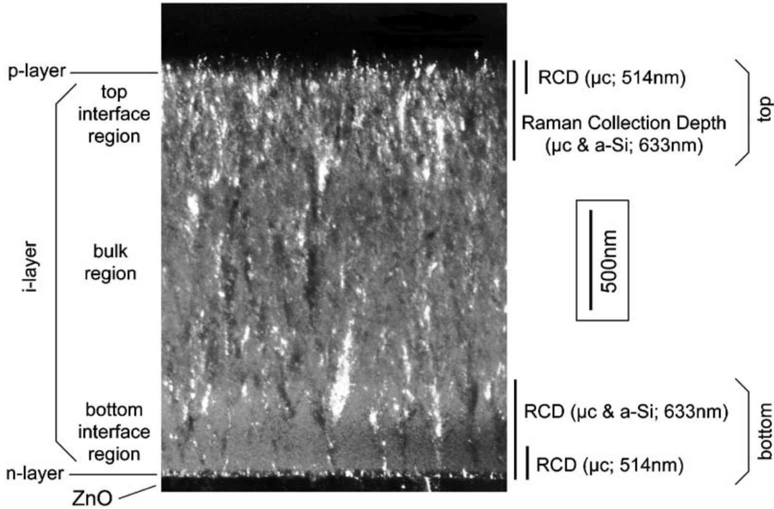

Fig. 2. TEM dark-field micrograph of the nip solar cell deposited with SC = 7% on sputtered ZnO (black layer at the bottom of the micrograph). The corresponding Raman spectra of this solar cell are given in Fig. 1. The n-doped μc-Si:H layer appears as a thin dotty layer (~ 30 nm thick) at the top of the ZnO. At the bottom of the i-layer, amorphous silicon appears uniformly grey, between conical conglomerates of nanocrystals. The latter is the microcrystalline silicon phase. After the coalescence of the microcrystalline cones, the amorphous material is no longer observable in this medium-resolution micrograph. The p-layer (at the top of the picture) is not distinguishable from the i-layer. The Raman collection depths (RCD) probed with our bifacial depth-dependent micro-Raman technique in a-Si:H and μc-Si:H, at 514 and 633 nm, respectively, are indicated. RCD is defined as $1/(2\alpha)$, where α is the absorption coefficient of the a-Si:H or μc-Si:H material at the considered wavelength. Note that the value of RCD at 514 nm for a-Si:H is about a third of the corresponding value for μc-Si:H.

schematically illustrated in Fig. 2. For the strongly absorbed excitation light (514 nm), the collected Raman contribution arises from the doped layer (~ 20–30 nm) and from the first tens of nanometres of the i-layer. On the other hand, for the weakly absorbed excitation light (633 nm), the collected Raman contribution arises from up to 500 nm below the illuminated surface and, thus, contains an important contribution from the i-layer (whose typical thickness is 2–2.5 μm), that is in this case much larger than the contribution from the doped layer.

As can be qualitatively seen from Fig. 1, the ratio of crystalline peak intensity to amorphous peak intensity continuously decreases from the top to the bottom of the device. This behaviour corresponds well to typical device microstructure (as seen e.g. in the TEM micrograph of Fig. 2), where the top of the cell is microcrystalline, whilst an important amorphous fraction is observed at the bottom of the device.

The crystalline volume fraction (X_c) of a sample deduced from its Raman spectrum is usually expressed as [18,19]:

$$X_c = I_c/(I_c + yI_a), \tag{1}$$

where I_c and I_a are the integrated Raman scattered intensities of the crystalline and amorphous parts, respectively, and $y = \Sigma_c/\Sigma_a$ is the ratio of the Raman diffusion

cross-section for c-Si over that of a-Si:H [18]. Whereas I_c and I_a can be directly measured from the Raman spectra, the value of y is still a matter of debate. Values from 0.88 [18] down to 0.1 [20] have been published. Furthermore, y depends on the size of the crystallites and on the excitation wavelength [19]. These are the reasons why we will use here the parameter ϕ_c called by us ‘‘Raman crystallinity factor’’ for which we arbitrarily set $y = 1$; this factor does not reflect the actual crystalline volume fraction, but is simply a ratio of Raman intensities that is calculated as follows:

$$\phi_c = (I_{520} + I_{510})/(I_{520} + I_{510} + I_{480}), \quad (2)$$

where I_i is the area under the Gaussian centred at i and $I_{520} + I_{510} + I_{480}$ is the total integrated intensity. The value of ϕ_c should be considered as a lower limit for the actual crystalline volume fraction [5].

Fig. 3a shows the values of ϕ_c evaluated from the deconvoluted spectra obtained with the bifacial depth-dependent Raman technique for the silane concentration series of nip-type solar cells deposited on sputtered ZnO. We observe that the different ϕ_c-values vary smoothly with the silane concentration of the i-layer. The slight discontinuity at 5.5%, especially visible in the n–i 514 nm curve, is due to a problem in the deposition sequence (involuntarily, a reduction of power was applied

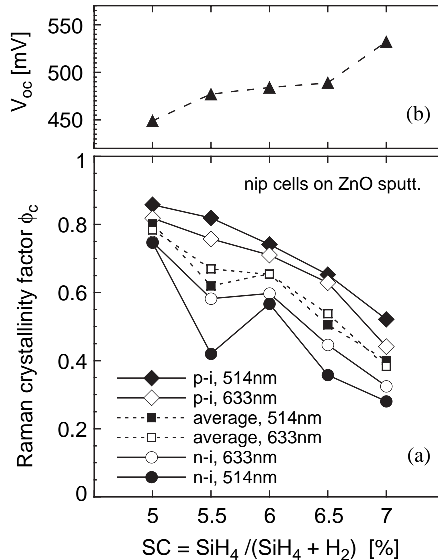

Fig. 3. (a) Raman crystallinity factors (ϕ_c) (see text) and (b) open circuit voltage (V_{oc}), for a series of nip solar cells deposited on sputtered ZnO, where the i-layer was deposited at various values of the silane concentration (SC) [8,9]. Measurements were performed with 514 nm (filled symbols) and 633 nm (open symbols) excitation light, from the top (p–i) side (diamond-like symbols) and from the bottom (n–i) side through the glass (circles). The spectra corresponding to the Raman crystallinity values of the 7% cell are those of Fig. 1. The average values of the top and bottom crystallinities are also represented (squares) for both excitation lights.

to the plasma at the beginning of the i-layer growth). In Fig. 3, the four curves are almost parallel: they show a continuous decrease of ϕ_c with increasing SC as used for i-layer deposition. The values of ϕ_c shown here are representative of the bottom n–i (less crystalline) and top p–i (more crystalline) parts of the cells; thereby, the crystallinity within the cell appears to increase as growth proceeds. This is confirmed by a TEM cross-section micrograph (Fig. 2) of the nip cell where the i-layer was deposited at SC = 7%. On this micrograph, conical conglomerates of nanocrystals start to grow from the n-layer onwards. Before the cones coalesce, they are embedded in amorphous silicon. The top of the device exhibits, in this micrograph, a good crystallinity, with little (or no) amorphous phase.

In Fig. 3a, the four values of ϕ_c are ordered in the same sequence for each SC: the ϕ_c-value for bottom illumination at 514 nm, which probes the beginning of growth (n–i part) of the solar cells, exhibits the lowest measured value as compared to the three other ϕ_c-values; after that follows the ϕ_c-value for bottom illumination at 633 nm, where we probe the same volume as in the preceding case plus a substantial (lower) part of the bulk of the i-layer, whose crystallinity increases with growth; afterwards, the ϕ_c-value for top illumination at 633 nm probes about the same volume as in the previous case but this time from the top, giving thus rise to superior values; finally, the ϕ_c-value for top illumination at 514 nm is the highest, although it is still very close to the preceding ϕ_c-value; indeed we are now probing the "last" part of the i-layer plus the p-layer that has grown epitaxially on the underlying i-layer.

In Fig. 3 we also show the algebraic average ϕ_c^A of the Raman crystallinity factors calculated as follows for each wavelength:

$$\phi_c^A = (\phi_c^{top} + \phi_c^{bottom})/2 \tag{3}$$

with $\phi_c^{top} = \phi_c^{p-i}$ and $\phi_c^{bottom} = \phi_c^{n-i}$ for the nip cells, and $\phi_c^{top} = \phi_c^{n-i}$ and $\phi_c^{bottom} = \phi_c^{p-i}$ for the pin cells (as used in Section 3.2).

Surprisingly, ϕ_c^A (SC) is similar for both wavelengths. This fact is partially explained by the presence of the highly microcrystalline n-doped layer that increases the measured Raman crystallinity factor at 514 nm evaluated within RCD of the bottom of the solar cell.

3.2. Link with electrical solar cell performances

An effect that is generally observed [4,21] when one increases the silane concentration used for the deposition of the i-layer is a steady increase in the V_{oc}, followed by an abrupt change close to the μc-Si:H/a-Si:H transition [7]. The evolution of V_{oc} with silane concentration for the nip series deposited on sputtered ZnO is given in Fig. 3b.

In order to establish a relationship between the Raman crystallinity factors and the electrical performances of the solar cells, the results of the measurements on both nip- and pin-type solar cells devices will be discussed below. When only one of the Raman crystallinity factors measured at 514 nm either on the n–i side (ϕ_c^{n-i}) or on the p–i side (ϕ_c^{p-i}) is used as monitor of the device material, a decrease in V_{oc} is

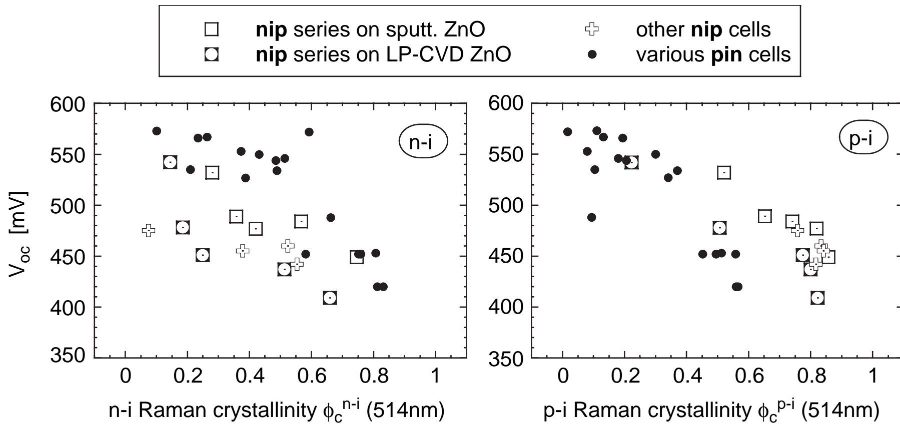

Fig. 4. Dependence of V_{oc} on the Raman crystallinity factor (ϕ_c) measured at 514 nm for two silane concentration series of nip-type solar cells, as well as for various other nip- and pin-type μc-Si:H solar cells. Left: V_{oc} as a function of ϕ_c^{n-i}, where ϕ_c^{n-i} is measured on the n–i side; Right: V_{oc} as a function of ϕ_c^{p-i}, where ϕ_c^{p-i} is measured on the p–i side. Note that the n–i side corresponds to the bottom (beginning of growth) of the nip cells and to the top (end of growth) of the pin cells, whereas the p–i side corresponds to the top (end of growth) of the nip cells and to the bottom (beginning of growth) of the pin cells.

observed with an increase in ϕ_c (Fig. 4 left and right, respectively). However, the scattering of the data set is quite pronounced, especially for the V_{oc} vs. ϕ_c^{n-i} case. On the other hand, when the average Raman crystallinity ϕ_c^A at 514 nm is used as monitor of the device material, a linear dependence of V_{oc} with ϕ_c^A is observed (Fig. 5). This linear increase observed for V_{oc} as ϕ_c^A decreases is indeed seen for both individual nip series (Fig. 5 open squares and open circles/squares), as well as for a large set of other solar cells, deposited in the nip- and pin-configurations in our laboratory, as also shown in Fig. 5 (all symbols).

Note that (as already stated) the Raman crystallinity factor used here is not a real crystalline volume fraction, because the Raman cross-section ratio has been arbitrarily set to $y = 1$ for the evaluation of the Raman crystallinity factor. However, even if we use values of y as given in the literature ($y \neq 1$) to define another crystallinity factor, we would still observe a roughly linear dependence of V_{oc} with this "new" ϕ_c^A: for example, with a value of $y = 0.88$ [18], the least-square linear fit still has a correlation coefficient of 0.89, whereas it decreases down to 0.79 if one uses the extreme value $y = 0.1$ [20]. On the other hand, even if the V_{oc} is plotted as a function of ϕ_c^A at 633 nm (instead of 514 nm), the trend observed in Fig. 5 is once again practically conserved.

In its definition and in the way ϕ_c^A is measured, this quantity includes the contributions of both doped and undoped layer crystallinities. Highly crystalline p-doped layers have been shown to be beneficial for the electrical performance of pin-type solar cells [22]. Indeed, such highly microcrystalline layers act as seeding layers for the microcrystalline growth of the i-layer; in fact these layers can also, in general, be very effectively doped, and their Fermi level pushed down to near the valence bandedge, this being a necessary condition for obtaining high values of the

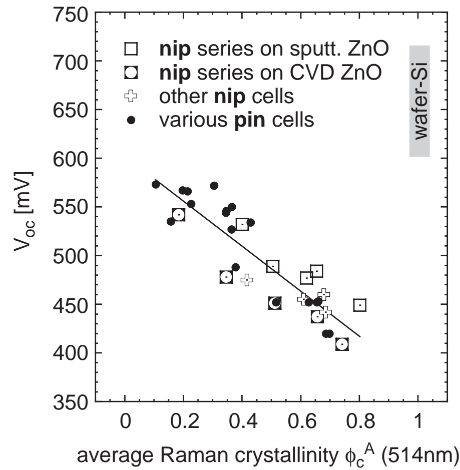

Fig. 5. Dependence of the open-circuit voltage (V_{oc}) of two silane concentration series of nip-type solar cells, as well as of various other nip- and pin-type μc-Si:H solar cells on the average Raman crystallinity factor (ϕ_c^A) (see text) measured at 514 nm. The full line is a linear fit using the least-squared error method where the linear correlation coefficient is $R = 0.89$. The range for V_{oc}-values obtained for wafer-based crystalline silicon solar cells is indicated; note that for amorphous silicon cells, V_{oc}-values reach a maximum of about 900 mV, for current, state-of-the-art solar cell technology.

built-in voltage and, thus, also a pre-condition for obtaining a high value of V_{oc}. In our case, the Raman probe beam always enters first the doped microcrystalline p- or n-layer. Then, it probes the initial region of the i-layer, starting with the interface region and then penetrating more or less deeply into the bulk of the i-layer (see Fig. 2), depending upon whether we use the 633 nm probe beam or the 514 nm probe beam. As both n–i and p–i junctions contribute to the building of the internal field in open-circuit conditions, ϕ_c^A takes indeed into account both contributions by averaging the crystallinity of the top and bottom parts of the cell.

From our measurements (see Figs. 4 and 5) it becomes clear that the interface regions have a major influence on the value of V_{oc}, and that it is the *average* crystallinity (factor) of the *two* interface regions that counts: the more amorphous-like these two interface regions are, on an average, the higher V_{oc} becomes. As the bulk of the i-layer also changes in crystallinity if SC is changed, we are, however, not yet able to say whether it is solely the interface region, as other experiments have suggested [23], or also the bulk material, as proposed in Ref. [24], that determine V_{oc}. To be able to discriminate here between these two hypothesis, further experiments would be necessary.

4. Conclusions

Bifacial micro-Raman spectroscopy has been carried out in actual, complete single junction μc-Si:H solar cells, on which electrical performances were also measured. It

turns out to be a very convenient non-destructive and fast technique that can be applied for monitoring the crystallinity at various depths in the device. Raman spectra obtained by this technique exhibit different relative intensities of the crystalline and amorphous line. This results from an inhomogeneous crystalline fraction within the device, and is indeed in good agreement with TEM micrograph.

As extracting the crystalline volume fraction from Raman spectra involves using the debated values of the scattering cross-sections for a-Si:H and c-Si, we have used here a ‘‘Raman crystallinity factor’’ for which the ratio of these scattering cross-sections is arbitrarily taken as being equal to one. We have identified the two Raman crystallinity factors which probe the regions close to the n–i and p–i interfaces, as constituting fundamental microstructural parameters for solar cell device characterisation, because they are directly related to the value of V_{oc}. Indeed, V_{oc} linearly decreases when the algebraic average of the top crystallinity and bottom crystallinity factors, as evaluated directly on entire solar cells, increases. This has been observed for a large set of solar cells representative of our in-house VHF-GD-based solar cell technology, for both nip- and pin-type solar cells. Nevertheless, further investigations are needed in order to identify more accurately the precise thickness of the solar cell region that is important for forming V_{oc}. One needs, also, to check whether the linear relation found above is still maintained for other deposition processes, such as RF-GD at 13.56 MHz or such as hot wire deposition.

Acknowledgements

The authors thank Dr. E. Bustarret from CNRS, Grenoble for his help in the preliminary experiments of this study. This work was supported by the Swiss National Science Foundation under grant FN59413 and FN66985, as well as by the Swiss Federal Office of Energy (OFEN) under contract No. 36487.

References

[1] E. Vallat-Sauvain, U. Kroll, J. Meier, A. Shah, J. Pohl, J. Appl. Phys. 87 (6) (2000) 3137.
[2] M. Luysberg, P. Hapke, R. Carius, F. Finger, Philos. Mag. A 75 (1997) 31.
[3] J. Bailat, E. Vallat-Sauvain, L. Feitknecht, C. Droz, A. Shah, J. Non-Cryst. Solids 299–302 (2002) 1219.
[4] J. Meier, E. Vallat-Sauvain, S. Dubail, U. Kroll, J. Dubail, S. Golay, L. Feitknecht, P. Torres, S. Faÿ, D. Fischer, A. Shah, Sol. Energy Mater. Sol. Cells 66 (2001) 73.
[5] L. Houben, M. Luysberg, P. Hapke, R. Carius, F. Finger, H. Wagner, Philos. Mag. A 77 (6) (1998) 1447.
[6] A. Shah, J. Meier, E. Vallat-Sauvain, C. Droz, U. Kroll, N. Wyrsch, J. Guillet, U. Graf, Thin Solid Films 403 (2002) 179.
[7] T. Roschek, T. Repmann, J. Muller, B. Rech, H. Wagner, J. Vac. Sci. Technol. A 20 (2) (2002) 492.
[8] J. Bailat, E. Vallat-Sauvain, L. Feitknecht, C. Droz, A. Shah, J. Appl. Phys. 93 (9) (2003) 5727.
[9] L. Feitknecht, O. Kluth, Y. Ziegler, X. Niquille, P. Torres, J. Meier, N. Wyrsch, A. Shah, Sol. Energy Mater. Sol. Cells 66 (2001) 397.
[10] J. Benedict, R. Andersen, S.J. Klepeis, Mater. Res. Soc. Symp. Proc. 254 (1992) 121.

[11] D.W. Marquardt, J. Soc. Ind. Appl. Math. 11 (2) (1963) 431.
[12] M.N. Islam, S. Kumar, Appl. Phys. Lett. 78 (6) (2001) 715.
[13] R.J. Kobliska, S.A. Solin, Phys. Rev. B 8 (1973) 3799.
[14] C. Droz, E. Vallat-Sauvain, J. Bailat, L. Feitknecht, A. Shah, Proceedings of the 17th European Photovoltaic Solar Energy Conference, Münich, Germany, 2001, p. 2917.
[15] Z. Hang, H. Shen, F.H. Pollak, J. Appl. Phys. 64 (6) (1988) 3233.
[16] N. Beck, J. Meier, J. Fric, Z. Remes, A. Poruba, R. Flückiger, J. Pohl, A. Shah, M. Vanecek, J. Non-Cryst. Solids 198–200 (1996) 903.
[17] V. Paillard, P. Puech, P.R.I. Cabarrocas, J. Non-Cryst. Solids 299–302 (2002) 280.
[18] R. Tsu, J. Gonzalez-Hernandez, S.S. Chao, S.C. Lee, K. Tanaka, Appl. Phys. Lett. 40 (6) (1982) 534.
[19] E. Bustarret, M.A. Hachicha, M. Brunel, Appl. Phys. Lett. 52 (20) (1988) 1675.
[20] M.H. Brodsky, M. Cardona, J.J. Coumo, Phys. Rev. B 16 (1977) 3556.
[21] S. Klein, F. Finger, R. Carius, B. Rech, L. Houben, M. Luysberg, M. Stutzmann, Mater. Res. Soc. Symp. Proc. 715 (2002) A26.2.1.
[22] E. Vallat-Sauvain, S. Faÿ, S. Dubail, J. Meier, J. Bailat, U. Kroll, A. Shah, Mater. Res. Soc. Symp. Proc. 664 (2001) A15.3.1.
[23] J. Meier, S. Dubail, J. Cuperus, U. Kroll, R. Platz, P. Torres, J.A.A. Selvan, P. Pernet, N. Beck, N.P. Vaucher, C. Hof, D. Fischer, H. Keppner, A. Shah, J. Non-Cryst. Solids 227–230 (1998) 1250.
[24] O. Vetterl, A. Lambertz, A. Dasgupta, F. Finger, B. Rech, O. Kluth, H. Wagner, Sol. Energy Mater. Sol. Cells 66 (1–4) (2001) 345.